Evaluation of Hybrid-Short-Coir-Fibre-Reinforced Composites via Full Factorial Design

Lívia Á. Oliveira[1], Júlio C. Santos[1], Túlio H. Panzera[1]*, Rodrigo T. S. Freire[2], Luciano M. G. Vieira[3], Fabrizio Scarpa[4]

[1]Centre for Innovation and Technology in Composite Materials, Department of Mechanical Engineering, Federal University of São João del Rei - UFSJ, São João del Rei, Minas Gerais, Brazil.

*Corresponding author: panzera@ufsj.edu.br

[2]Centre for Innovation and Technology in Composite Materials, Department of Natural Science, Federal University of São João del Rei - UFSJ, São João del Rei, Minas Gerais, Brazil.

[3]Departament of Production Engineering, Federal University of Minas Gerais - UFMG, Belo Horizonte, Minas Gerais, Brazil.

[4]Bristol Composites Institute (ACCIS), University of Bristol, UK.

Abstract

A full factorial design ($2^2 3^1$) has been used to investigate the effect of the use of sodium hydroxide fibre treatment, Portland cement and uniaxial pressure on the physical and mechanical properties of hybrid short coir fibre reinforced composites (HSCoirFRCs). The response variables considered in this work were the apparent density, porosity, tensile and flexural strength, the modulus of elasticity and the Charpy impact resistance. The alkali treatment contributed not only to reduce the apparent porosity, but also to increase the mechanical properties of the HSCoirFRCs. A reduction of the impact resistance and an increase of the apparent density was also identified after treatment. Cold pressing significantly affected the physical and mechanical properties of the HSCoirFRCs. Higher pressure levels enhanced the wettability of the fibres and, consequently, the mechanical performance of the composites. The incorporation of cement microparticles as a second reinforcement phase was however not effective, leading to decreased strength and an increased apparent density of the materials. The HSCoirFRC structure can be considered an economical and sustainable alternative for future secondary structural parts in lightweight transport applications.

Keywords: coir fibre; hybrid composites; full factorial design; alkaline treatment; Portland cement; compaction.

1. Introduction

In recent years, the rapidly expanding use of composite components in automotive, aerospace, construction, sports, leisure, packaging and other mass production industries has considerably raised the need for sustainable and renewable reinforced composites [1, 2]. As a result, the demand for natural fibres as polymer composite reinforcements has drastically increased over the past few years due to their intrinsic advantages over synthetic fibres such as: low cost, low density, availability, biodegradability, recyclability, easy processing and moderate mechanical performance [3-9].

Advances regarding the use of natural fibre reinforced polymer composites in automotive and construction engineering have been achieved in recent years. Yan and Chouw [10] have studied the crashworthiness characteristics of natural fibre reinforced epoxy tubes as an energy absorber for automotive applications. This composite revealed to be a useful energy absorber device under compressive loads. Similar research was conducted by Yan et al. [11], which investigated the crashworthiness characteristics of empty and polyurethane-foam filled natural flax fabric reinforced epoxy composite tubes under quasi-static lateral compression. In a specific design, these tubes were similar to aluminium and glass/carbon fibre reinforced composite tubes as energy absorbers. In civil or transport engineering, the developed composites achieved acceptable properties to be used as rail along roads and, in automotive engineering, as roll bars in buses or frontal crushed tubes in a vehicle for crashworthiness proposal. Yan and Chouw [12] have investigated the feasibility of natural flax fabric reinforced epoxy composite tube encased coir fibre reinforced concrete (FFRP-CFRC), a composite column for structural applications. The findings revealed that the material can be used as sustainable structural members for axial and flexural loadings. Huang et al. [13] have investigated the flexural behaviour of reinforced concrete beams strengthened with externally bonded natural flax fibre-reinforced plates (FFRP) under four-point bending test. In general, FFRP composites can be considered an environmentally-friendly external reinforcement material to retrofit and/or strengthen deficiently-designed and/or damaged reinforced concrete structures after earthquakes.

Among natural fibres, coir is widely used in yard and rope manufacturing, as well as in producing floor-furnishing materials. Coir is a low cost, durable, versatile and abundant material [14-16]. The fibre is extracted from the husk of the coconut fruit palm (*Cocos nucifera*), which is extensively cultivated in tropical regions such as

Brazil, India, Sri Lanka and Southeast Asia [14, 17, 18]. Fifty-five billion coconuts are produced every year, and just a small fraction of them are recovered for use. Most husks are disposed of, causing environmental pollution issues [19, 20]. Therefore, research and development efforts have been underway to find new applications for coir. Polymer composite reinforcements represent a natural way to exploit the properties of coir, because of its resilience, high elongation at break, weather, fungal and bacterial resistance and considerable toughness [20-23]. The main limitation of natural fibre reinforcement lies however in the incompatibility between (hydrophilic) fibres and (hydrophobic) polymeric matrices. Several treatments have been proposed to chemically modify the surface of fibres and enhance the fibre-matrix adhesion [22-24]. Among these, alkaline treatments represent the most effective and economical technique for coir [25, 26].

Another strategy to enhance the properties of laminated composites and specifically to increase their thermal stability and stiffness is the embedding of micron-sized fillers like ceramic minerals into the matrix [27-29]. According to Silva et al. [30] particles can function as barriers against crack propagation due to their high stiffness, which delays crack growth in hybrid composites and increases their mechanical properties.

Therefore, the present work investigates the feasibility of hybrid-short-coir-fibre-reinforced composites (HSCoirFRC) as a sustainable, low cost and acceptable mechanical performance material for secondary structural components in engineering applications. In addition, the effects provided by the coir fibre alkali treatment, the inclusion of cement microparticles and the uniaxial compaction over the physical and mechanical properties of HSCoirFRCs were evaluated through a statistical full factorial design.

2. Materials and Methods

2.1 Materials

The matrix used in the composites was obtained by mixing epoxy resin of the type Renlam M and hardener HY956 supplied by Huntsman (São Paulo – Brazil), with a 5:1 (wt/wt) proportion. Coir fibres were supplied by *Deflor Bioengenharia* (Belo Horizonte – Brazil). The matrix was modified by incorporating white Portland cement microparticles (see composition in Table 1) obtained from Cemex Company (Mexico). The particles were classified by sieving within a particle size range of 37

μm – 44 μm. Sodium hydroxide (NaOH, 99%) was used to treat the fibres, the latter sourced from *Sulfal Química* (Belo Horizonte – Brazil).

Table 1. Chemical composition of white Portland cement

White Portland cement composition (%)	
SiO_2	22.48
Al_2O_3	7.52
Fe_2O_3	2.59
CaO	56.85
MgO	2.96
SO_3	1.55
Na_2O	0.29
K_2O	0.87
CO_2	4.89

2.2 Coir fibre treatment

Coir fibres in pristine conditions were manually cleaned for the complete removal of plant debris and coarse residues, such as coconut husks (Figure 1a). Subsequently, the fibres were immersed in a 10 wt% solution of sodium hydroxide at room temperature for 15 hours (Figure 1b) and then washed in fresh water for several times to remove any excess of NaOH from the fibres. Finally, the treated coir fibres were oven-dried at 60°C for 72h and sealed in a plastic bag to avoid moisture absorption until being used as a dispersive phase of the polymeric composites (Figure 1c).

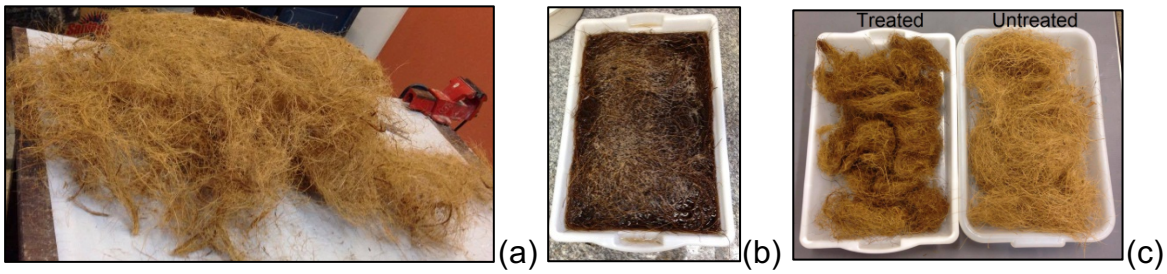

(a) (b) (c)

Figure 1. Coir fibres: (a) in pristine condition, (b) under sodium hydroxide treatment, (c) ready to be used as a reinforcing material.

2.3 Design of experiments

A full factorial design ($2^2 3^1$) was established to investigate the effect of fibre chemical treatment (treated/untreated), cement inclusion (0/5/10 wt%) and uniaxial

pressure (490/654 kPa) on the physical and mechanical properties of the HSCoirFRC composites. The design resulted in 12 experimental conditions, as shown in Table 2.

Table 2. Full factorial design ($2^2 3^1$).

Experimental Condition	Chemical Treatment	Cement Inclusion (wt%)	Uniaxial Pressure (kPa)
1	Untreated	0a	490
2	Untreated	0	654
3	Untreated	5	490
4	Untreated	5	654
5	Untreated	10	490
6	Untreated	10	654
7	Treated	0	490
8	Treated	0	654
9	Treated	5	490
10	Treated	5	654
11	Treated	10	490
12	Treated	10	654

The chemical treatment factor was established in order to increase fibre-matrix adhesion and, consequently, the mechanical properties of the composites. The cement inclusion factor was used to enhance the matrix stiffness. The factor and levels were selected based on previous work conducted by this research group [31-33]. The uniaxial pressure was used to improve the fibres wettability and the composite surface finish. The pressure levels were determined based on preliminary tests. The lower level, 490 kPa, corresponds to 4.5 tons, while the upper level, 654 kPa, corresponds to 6 tons.

The manufacturing parameters that were kept constant during the experiment were the type of matrix (epoxy resin/HY956 hardener), the fibre grammage per layer (300 g/m^2), the number of fibre layers per composite plate (3 layers), the cold-pressing time (22 hours) and the curing time (28 days). The factors, levels and parameters were set based on preliminary tests [34].

The responses investigated during the experiments were the apparent density, the apparent porosity, the mechanical strength, the modulus under tensile and flexural loading, and the Charpy impact resistance.

Twenty specimens (5 for each test: physical, tensile, bending and impact tests) were fabricated for each experimental condition. Two replicates were also considered, running a total of 480 specimens. A randomization procedure was adopted during the fabrication of the samples and tests to avoid the effects provided by non-controlled factors on the responses. The statistical software Minitab 16 was used to perform the Design of Experiments (DoE) and Analysis of Variance (ANOVA) techniques.

2.4 Manufacturing process

The fabrication of the composite materials was carried out via hand lay-up technique (Figure 2). A metallic mould with dimensions of 300 x 300 mm was used to compact the samples (Figure 2a). Coir fibres (in pristine and treated conditions), ranging from around 20 to 180 mm in length, were weighted according to the required grammage (300 g/m^2) and randomly distributed inside the mould. A preliminary uniaxial pressure of 654 kPa was applied for 2 minutes to obtain a randomly oriented coir fibre fabric (Figure 2b). An aluminium plate (Figure 2c), covered with a thin layer of wax as releasing agent, was placed inside the mould to provide a good surface finish. The polymeric matrix was prepared by combining firstly the resin and the hardener; afterwards the microparticles were added and hand-mixed by 5 minutes at room temperature (~23 ^oC) to ensure a good dispersion/distribution of cement particles into the matrix phase. Three fabrics were assembled inside the mould and the polymeric matrix (modified and non-modified) was uniformly spread on the fibres (Figure 2d). Two levels of pressure (490 and 654 kPa) were used to produce the samples (Figure 2e). After 22 hours under pressure, the material was removed from the mould (Figure 2f) and placed in a plastic container to avoid moisture absorption during 28 curing days. Finally, the composite plate was cut (Figure 2g) according to the recommendations of the ASTM standards and tested.

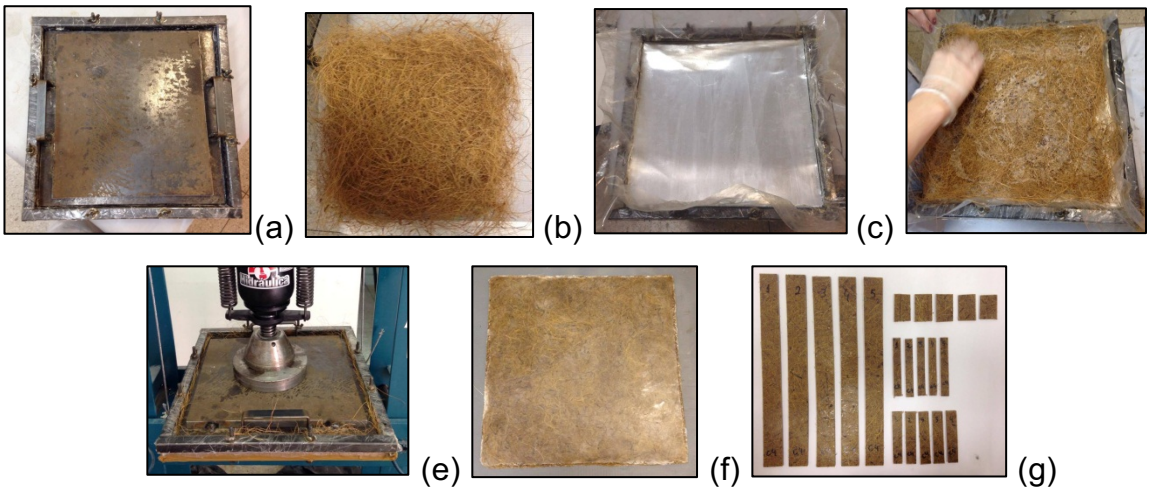

Figure 2. Fabrication process of the composites: (a) metallic mould, (b) fabric of random coir fibres, (c) aluminium plate, (d) fabric arranged inside the mould, (e) cold pressing, (f) composite plate and (g) specimens for testing.

2.5 Characterization of the phases

The mechanical properties of the untreated and treated coir fibres were determined through tensile testing carried out according to ASTM D3822-14 [35]. A single fibre was glued on a paper and clamped on a universal testing machine. A constant cross-section was assumed to estimate the tensile properties, and a crosshead speed of 5 mm/min was considered during the tests. Fifteen samples of each condition (treated and untreated) were tested. The physical properties of the fibres were determined by using apparent density test, following the Archimedes principle and the ASTM D276-12 standard [36]. The thermal stability of the fibres was evaluated by thermogravimetric analysis (TGA) using a Shimadzu DTG-60. The samples were heated from room temperature to 800^{o}C at a heating rate of 20 ^{o}C/min and a nitrogen gas flow rate of 50 mL/min. A scanning electron microscope (SEM) Hitachi T-3000 was used to observe the microstructure of the coir fibres and the cross section of the composite specimens.

The matrix phase (modified and non-modified) was subjected to tensile, flexural and compressive tests by using a Shimadzu AG-X Plus testing machine (with a 100 kN load cell), according to ASTM D638-14 [37], ASTM D790-15 [38] and ASTM D695-15 [39], respectively. The impact test was conducted according to ASTM D6110-10 [40]. The apparent density was also determined following the Archimedes principle. Five specimens were tested for each experimental condition.

2.6 Composites characterization

Tensile (Figure 3a) and flexural (Figure 3b) tests were carried out based on the recommendations of ASTM D3039-14 [41] and ASTM D790-15 [38], respectively. A Shimadzu AG-XPlus testing machine equipped with a 100 kN load cell was used to perform both tests, at a crosshead speed of 2 mm/min. Impact tests were carried out on a Charpy Impact Tester XJJ Series (Figure 3c), following the recommendations of the ASTM D6110-10 protocol [40]. The apparent density and porosity were determined according to the Archimedes principle using a desiccator coupled to a vacuum pump (Figure 3d), a precision balance (0.001g) (Figure 3e) and distilled water.

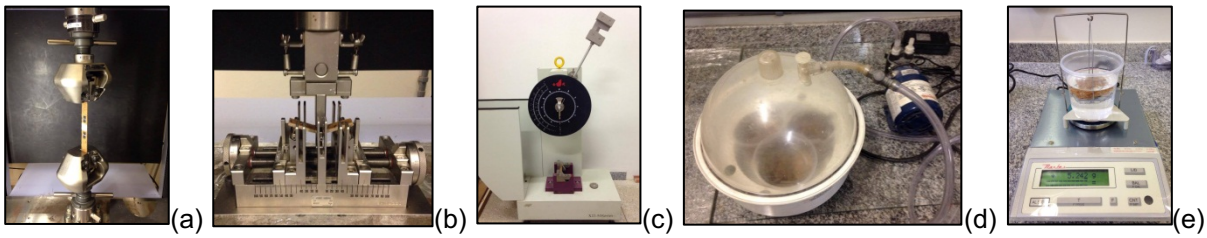

Figure 3. Equipment used in: (a) tensile, (b) flexural and (c) impact tests. Equipment used in physical tests: (d) pump-coupled vacuum desiccator and (e) precision balance.

3. Results and Discussion

3.1 Dispersive phase

Table 3 displays the experimental values for the physical and mechanical properties for treated and untreated coir fibres along with a set of values reported in the literature. These data are consistent with the measured results present in open literature for untreated fibres, except for the modulus of elasticity. According to Defoirdt et al. [43], as the coir fibre is a natural product, its properties depend not only on the plant species, but also on the climate and terrain where it has grown, harvest period, extraction method, the date of harvesting and the maturity at harvesting. Literature values for treated fibres were not compared due to the scarcity of data concerning the same treatment conditions used in this work. Some authors have, however, reported an increase in tensile strength, modulus of elasticity and elongation at break after the alkaline treatment, as observed in Table 3 [20, 45].

According to Van de Weyenberg et al. [25], sodium hydroxide can induce large lattice transformations in the cellulose components inside the plant fibre and also significantly removes the non-cellulosic (hemicellulose, lignin and pectin) constituents, allowing the cellulose fibrils to rearrange, decreasing the spiral angle and increasing the molecular orientation. This phenomenon leads to a better load distribution and higher ultimate stress achieved by the fibres.

Table 3. Coir fibre properties.

Property	Untreated fibre		Treated fibre
	Measurement	Literature	Measurement
Diameter (μm)	125 – 295	100 – 400 [6, 9, 42]	136 – 315
Apparent Density (g/cm^3)	0.86 ± 0.02	0.87 – 1.4 [2, 4, 42-44]	1.27 ± 0.05
Tensile Strength (MPa)	75 – 117	59 – 593 [2, 17, 42, 45]	114 – 170
Modulus of Elasticity (GPa)	0.85 – 1.71	2.7 – 6 [2, 17, 23, 43]	2.44 – 4.77
Elongation at break (%)	15 – 29	15 – 50 [7, 9, 23, 46]	19 – 34

Figure 4 shows the typical mechanical behaviour obtained for treated and untreated coir fibres under tensile loadings. The curves present the same behaviour, exhibiting a linear portion at low stresses, followed by a plastic region with some fraying effects, resulting on a large elongation at break. This non-linear nature of the stress–strain curve might be attributed to the successive rupture of the microfibrils. When the fibre is under tensile load, the stress levels are distinct along the microfibrils. Once a microfibril at the maximum stress breaks, the remaining microfibrils absorb the tension load and the stress starts increasing again as the fibre is deformed. This fact might be attributed to the rearrangement of the remaining cellulose fibrils under strain; the spiral angle is decreased while the molecular orientation is increased. This sudden enhancement in the coir fibre stress under high strain has been reported in the open literature [6, 44].

The mean stiffness values for treated and untreated coir fibre were 3.15 GPa and 1.67 GPa, respectively. The mean tensile strength (UTS) values for treated and untreated coir fibre were 125 MPa and 90 MPa, respectively. These findings reveal a significant post-treatment improvement in stiffness and strength of coir fibres after treatment.

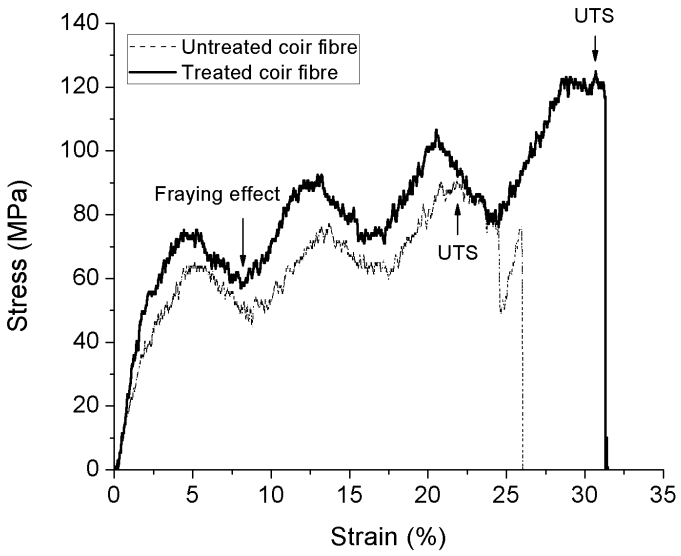

Figure 4. Stress/strain curve for coir fibre in tensile test.

Figure 5 shows the backscattering electron images of coir fibres in pristine (Figure 5a) and treated (Figure 5b) conditions with a magnification of 500×. The surface of untreated fibres reveals a large amount of impurities, waxes and debris. After treatment, it was observed an increase of voids and roughness owing to higher exposition of fibrils, with a resulting increase in the contact area. The results from Thermogravimetric analyses (TGA) also imply the removal of wax, pectin, lignin and hemicellulose from the fibre surface (Figure 6).

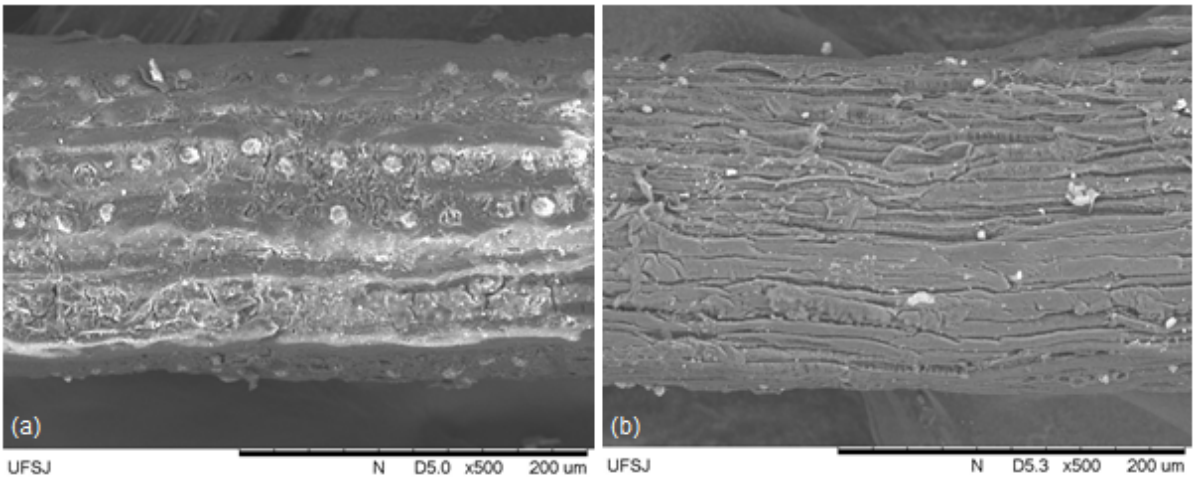

Figure 5. Untreated (a) and treated (b) coir fibre SEM images.

From the thermogravimetric curves one can observe the presence of three peaks, which characterize the fibre decomposition profile. The first one that is

characteristic of both fibres is attributed to the evaporation of water and occurs between room temperature and 150ºC. The second one (250 – 310ºC) is associated to the thermal degradation of the hemicellulose, while the third peak (310 – 400ºC) corresponds to the degradation of cellulose [47, 48]. Lignin presents a broad peak throughout the range, degrading between 225 to 500ºC [47, 49]. The decrease in the intensity of these peaks for treated fibres is a further testimony of the efficiency provided by the alkaline treatment to eliminate the superficial non-cellulosic compounds. The TGA/DTG results also show that the alkaline treatment decreased the range of the thermal stability for the fibres (333/303ºC for untreated fibre and 326/283ºC for treated specimens). The same behaviour has been also reported by Silva et al. with a similar alkaline treatment applied to coir fibres [45].

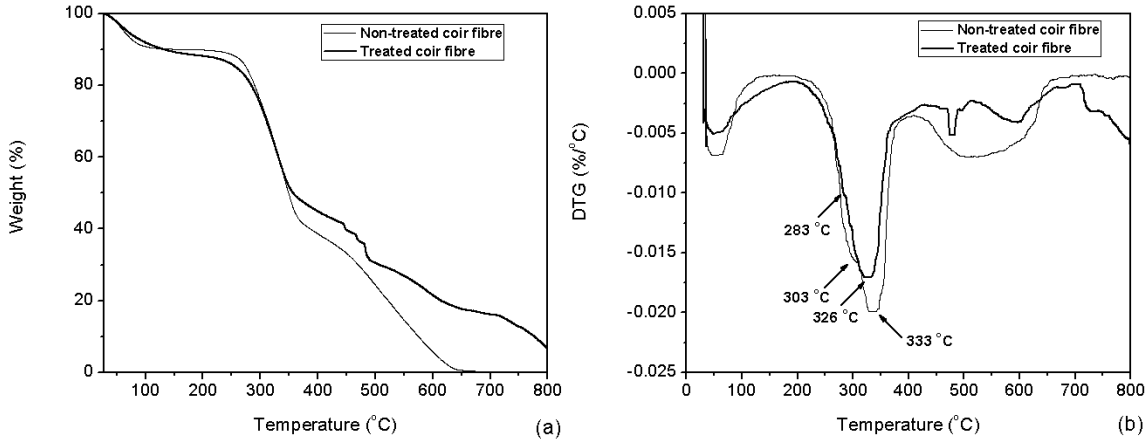

Figure 6. TGA (a) and DTG (b) curves for untreated and treated coir fibres.

3.2 Matrix

Figure 7 shows the SEM image of the cross-section composite after impact test. The image indicates a good dispersion of cement microparticles, represented by white dots.

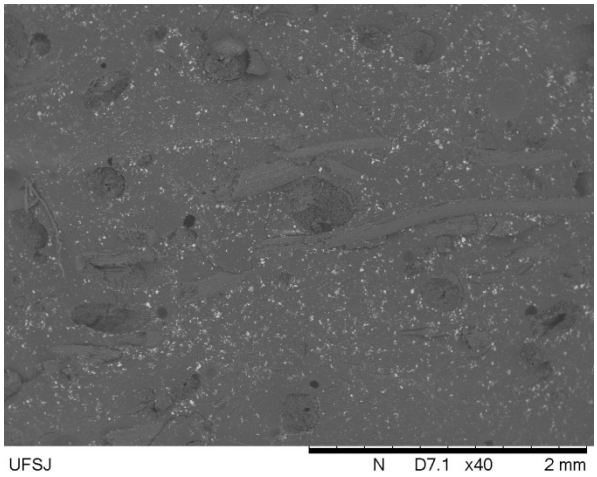

Figure 7. SEM image of the composite cross section.

Table 4 presents the physical and mechanical properties of the epoxy resin in pristine condition and modified with the white Portland cement microparticles. The dispersion of cement led to an increased density due to the higher density of such particulate phase (2.8 – 3.2 g/cm^3). The incorporation of the microparticles led to a decrease of the mechanical strength of the matrix, which can be attributed to the weak particle-matrix interfacial adhesion. On the other hand, the moduli increased due to the high stiffness of the cement microparticles. The reduction in impact resistance can be attributed to the increased brittleness caused by the presence of rigid particles.

Table 4. Properties of modified and non-modified matrices.

Property (Unit)		Type of matrix		
		0 wt.%	5 wt.%	10 wt.%
Apparent	Density (g/cm^3)	1.166 (±0.001)	1.201 (±0.003)	1.231 (±0.001)
Tensile	Strength (MPa)	4.8 (±2.5)	35.8 (±1.4)	30.4 (±1.7)
	Modulus (GPa)	1.92 (±0.11)	2.02 (±0.11)	2.04 (±0.10)
Flexural	Strength (MPa)	67.9 (±1.4)	64.8 (±1.4)	63.8 (±2.0)
	Modulus (GPa)	1.86 (±0.09)	2.04 (±0.19)	2.26 (±0.11)
Compression	Strength (MPa)	75.5 (±1.7)	74.1 (±1.2)	73.9 (±1.7)
	Modulus (GPa)	2.01 (±0.12)	2.12 (±0.06)	2.39 (±0.16)
Impact	Resistance (kJ/m^2)	8.7 (±1.4)	6.1 (±0.4)	5.8 (±0.8)

Figure 8 shows a comparison of the mechanical behaviour under tensile loading for the modified and non-modified matrices and composites in pristine condition (untreated fibre, non-modified matrix). A similar stress/strain curve is

observed for all conditions. The presence of the microparticles provided a slight increase in stiffness and a reduction in strength (Table 4). The mechanical strength of the coir fibre reinforced composites was significantly reduced in comparison to the one provided by the samples made from pure matrix only. This behaviour is attributed to the short length and the random orientation of the coir fibres, which prejudiced the load distribution along the fibre direction.

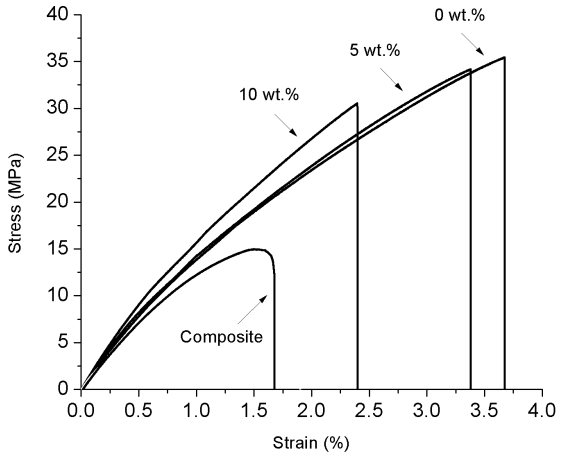

Figure 8. Representative stress/strain curve for modified and non-modified matrices and for the composites.

3.3 Statistical results

In order to investigate the effects of the factors CP, CT and CI and their interactions, it is necessary to evaluate the contribution of each factor or interaction on the response considered, which is done partitioning the total sum of squares, defined by $SS_T = \sum_i^a \sum_j^b \sum_l^c \sum_k^r (y_{ijlk} - \bar{y}_{....})^2$. The dot replacing a given index stands for the summation over that index, so that $y_{....} = \sum_i^a \sum_j^b \sum_l^c \sum_k^r y_{ijlk}$ and $\bar{y}_{....} = \frac{y_{....}}{abcr}$ represents the average over all the observations done.

The total sum of squares can be rewritten, after some algebra, as:

$$SS_T = SS_{CP} + SS_{CT} + SS_{CI} + SS_{CP \cdot CT} + SS_{CP \cdot CI} + SS_{CT \cdot CI} + SS_{CP \cdot CT \cdot CI} + SS_E \quad (1)$$

The first three terms stand for the sum of squares associated with the effect of each main factor, the next four terms stand for the interactions among the factors and the last term is the stochastic error, calculated for the *r* replicates within a given (i,j,l)th level of the factors. The so-called Mean Squares (MS) are defined as the Sum

of Squares divided by the respective number of Degrees of Freedom. The F-value for a given main effect or interaction is then defined as the ratio of the respective Mean Square and the Mean Square of the error. All this information is conveniently summarized in Table 5 for the three-factor ANOVA.

Table 5: Basic statistical quantities for the three-factor ANOVA

Sum of Squares	Mean Square	F
$SS_{CP} = \frac{1}{bcr}\sum_{i}^{a} y_{i\cdots}^2 - \frac{y_{\cdots}^2}{abcr}$	$MS_{CP} = \frac{SS_{CP}}{a-1}$	$\frac{MS_{CP}}{MS_E}$
$SS_{CT} = \frac{1}{acr}\sum_{j}^{b} y_{\cdot j\cdot}^2 - \frac{y_{\cdots}^2}{abcr}$	$MS_{CT} = \frac{SS_{CT}}{b-1}$	$\frac{MS_{CT}}{MS_E}$
$SS_{CI} = \frac{1}{abr}\sum_{l}^{c} y_{\cdot\cdot l}^2 - \frac{y_{\cdots}^2}{abcr}$	$MS_{CI} = \frac{SS_{CI}}{c-1}$	$\frac{MS_{CI}}{MS_E}$
$SS_{CP\cdot CT} = \frac{1}{cr}\sum_{i}^{a}\sum_{j}^{b} y_{ij\cdot}^2 - \frac{\bar{y}_{\cdots}}{abcr} - SS_{CP} - SS_{CT}$	$MS_{CP\cdot CT} = \frac{SS_{CP\cdot CT}}{(a-1)(b-1)}$	$\frac{MS_{\mathrm{CP}\square\mathrm{CT}}}{MS_E}$
$SS_{CP\cdot CI} = \frac{1}{br}\sum_{i}^{a}\sum_{l}^{c} y_{i\cdot l}^2 - \frac{\bar{y}_{\cdots}}{abcr} - SS_{CP} - SS_{CI}$	$MS_{CP\cdot CI} = \frac{SS_{CP\cdot CI}}{(a-1)(c-1)}$	$\frac{MS_{\mathrm{CP}\square\mathrm{CI}}}{MS_E}$
$SS_{CT\cdot CI} = \frac{1}{ar}\sum_{j}^{b}\sum_{l}^{c} y_{\cdot jl}^2 - \frac{\bar{y}_{\cdots}}{abcr} - SS_{CT} - SS_{CI}$	$MS_{CP\cdot CI} = \frac{SS_{CT\cdot CI}}{(b-1)(c-1)}$	$\frac{MS_{\mathrm{CT}\square\mathrm{CI}}}{MS_E}$
$SS_{CP\cdot CT\cdot CI} = \frac{1}{r}\sum_{i}^{a}\sum_{j}^{b}\sum_{l}^{c} y_{ijl\cdot}^2 - \frac{\bar{y}_{\cdots}}{abcr} - SS_{CP} - SS_{CT} - SS_{CI} - SS_{CP\cdot CT} - SS_{CT\cdot CI} - SS_{CP\cdot CI}$	$MS_{CP\cdot CI} = \frac{SS_{CP\cdot CT\cdot CI}}{(a-1)(b-1)(c-1)}$	$\frac{MS_{\mathrm{CP}\square\mathrm{CT}\square\mathrm{CI}}}{MS_E}$
$SS_E =$	$MS_E = \frac{SS_E}{abc(r-1)}$	

$SS_T - SS_{CP} - SS_{CT} - SS_{CI} - SS_{CP \cdot CT} - SS_{CT \cdot CI} - SS_{CP \cdot CI} - SS_{CP \cdot CT \cdot CI}$		

It is important to note that the expected value of a Mean Square is the variance of the error plus a term associated with the main effect or interaction of factors, so that should a null hypothesis be true, the variance (i.e., the expected value of the respective Mean Square) equals the variance of the stochastic error, since the effect of the main factor (or interaction) is zero. In this case, F = 1 and the effect caused by a given factor or interaction is not significantly higher than the effect caused by mere chance. Thus, the higher the value of F, the more significant the effect of a given factor, beyond any mere stochastic effect. Moreover, such significance can be statistically tested since, if a null hypothesis is true, the respective F value follows the Fisher-Snedecor probability density function F(d_1, d_2), which depends on the degrees of freedom of the numerator (d_1) and of the denominator (d_2) of F [50]. The P-value, which is the risk of rejecting the null hypotheses (no effect from the main factor or interaction) when the null hypothesis is in fact true, is then calculated as the area (probability) under the F(d_1, d_2) distribution that lies beyond the computed value of F. In this work, the effect is considered statistically significant for $P \leq 0.05$ [51].

Table 6 shows the ANOVA results related to the responses of the full-factorial design. The main effect of a factor should be only interpreted individually if there is no other evidence of interactions among factors [51]. P-values lower than 0.05 are underlined in Table 6, and those in bold letters will be interpreted via effect plots, which illustrate the statistical analysis and provide the variation of the significant effects. Larger values of R^2-adj (adjusted) indicate models of greater predictive ability [51]. The R^2-adj values obtained in the experiments varied from 86.53% to 98.53%, which are considered acceptable for ANOVA validation.

1

Table 6. Analysis of Variance (ANOVA)

ANOVA		P-value ≤ 0.05						
	Experimental Factors	Apparent density (g/cm^3)	Apparent Porosity (%)	Tensile Strength (MPa)	Modulus of Elasticity (GPa)	Flexural Strength (MPa)	Flexural Modulus (GPa)	Impact Resistance (kJ/m^2)
Main Factors	Compaction Pressure (CP)	0.844	0.955	0.097	0.021	0.170	0.000	0.018
	Cement Inclusion (CI)	0.000	0.658	0.007	**0.023**	0.002	0.131	0.650
	Chemical Treatment (CT)	0.000	0.000	0.000	0.000	0.000	0.000	0.000
Interactions	CP x CI	**0.006**	0.414	**0.008**	0.483	0.280	0.000	0.000
	CP x CT	0.995	**0.002**	0.106	**0.014**	0.050	0.006	0.165
	CI x CT	**0.006**	**0.000**	**0.047**	0.847	0.002	0.011	0.966
	CP x CI x CT	0.560	0.068	0.655	0.055	**0.000**	**0.000**	**0.000**
	R^2 - adj	98.53%	88.69%	95.55%	86.53%	96.90%	96.95%	88.74%
	P-value (Anderson Darling) ≥ 0.05	0.311	0.274	0.939	0.989	0.148	0.268	0.299

The ANOVA can be also validated through the residual plots when the residuals are well distributed along the straight line. In this case, P-values for Anderson-Darling normality test that are higher or equal to 0.05 imply that the data follow a normal distribution. Figure 9 shows the residual plot for the apparent density response. The residual plots for all responses revealed a similar behaviour, exhibiting P-values higher than 0.05 (see Anderson-Darling in Table 6). Therefore, the graphics for the other responses will not be presented in this paper.

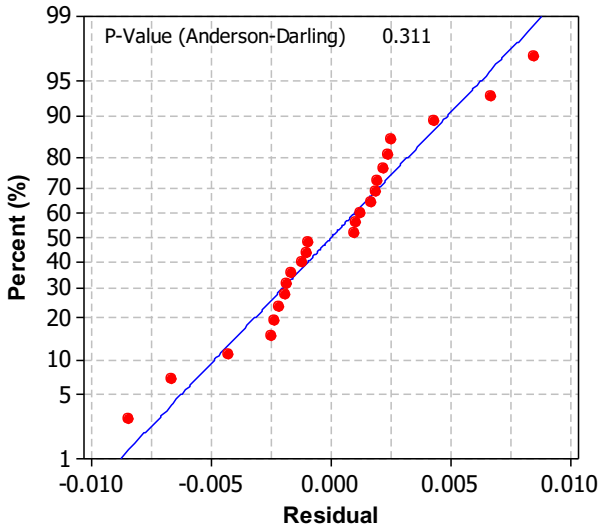

Figure 9. Residual plot for the apparent density of the composites.

Apparent Density

Figure 10 displays the second-order interaction effect plots for the mean apparent density response. The letters in blue represent the Tukey's comparison test, in which similar letters belong to the same grouping, i.e., equivalent means.

The presence of cement inclusions gradually increased the apparent density of the composites (Figures 10a and 10b) because of the superior density of these microparticles (2.8 – 3.2 g/cm^3). A slight variation in density was observed when the pressure changed from 490 kPa to 654 kPa (Figure 10a). However, the Tukey test shows equivalent means (similar grouping AA, BB and CC), indicating no significant changes on this response. Figure 10b reveals an increase of the mean of the apparent density in those composites fabricated with the treated fibres. This feature can be explained by the higher density of the coir after the alkaline treatment (1.27 g/cm^3).

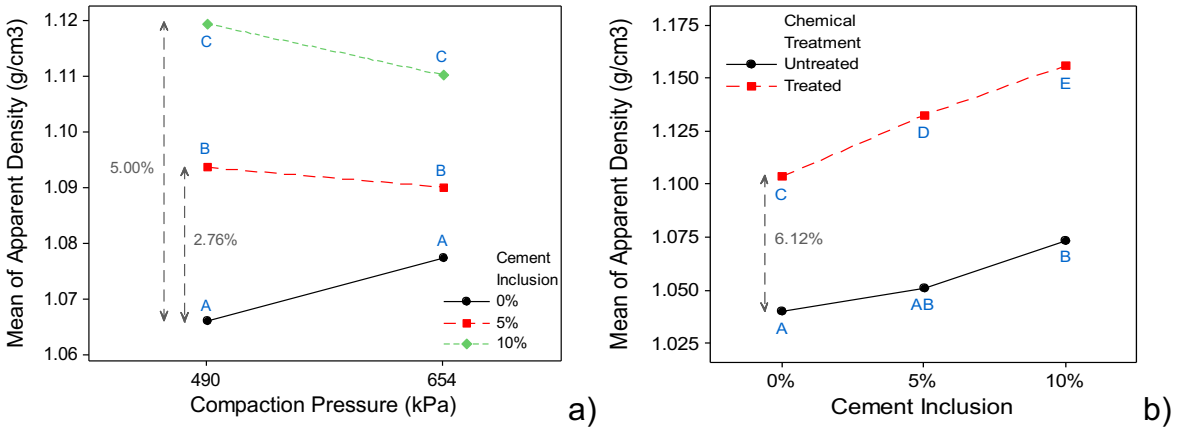

Figure 10. Second-order interaction effect plots for the mean apparent density response.

Apparent Porosity

Figure 11 shows the second-order interaction effect plots related to mean of the apparent porosity. The fibre contact area is increased due to the removal of non-cellulosic constituents (recall Figure 5), which contributes to the matrix phase infiltration [25]. Untreated coir fibre composites revealed a reduction of 10.33% in the apparent porosity when the higher-pressure level (654 kPa) was applied, which implies a better fibre wettability at higher compaction. In contrast, treated coir fibre composites revealed an increment of 15.25% in porosity at the higher pressing level. This behaviour is attributed to the presence of a higher fibre-volume fraction, since the fibres are more porous than the matrix and the amount of resin expelled out the mould in the case of the treated fibres is higher (see Table 7). In Figure 11b the cement inclusions provided a gradual increase of the porosity of the untreated composites due to the high viscosity of the polymer after particle incorporation, making the wettability of the fibres more difficult during the manufacturing process. The opposite effect was however observed in the case of the treated fibre composites, which implies that the cement particles were able to fill the voids on the fibre surface formed by the NaOH treatment.

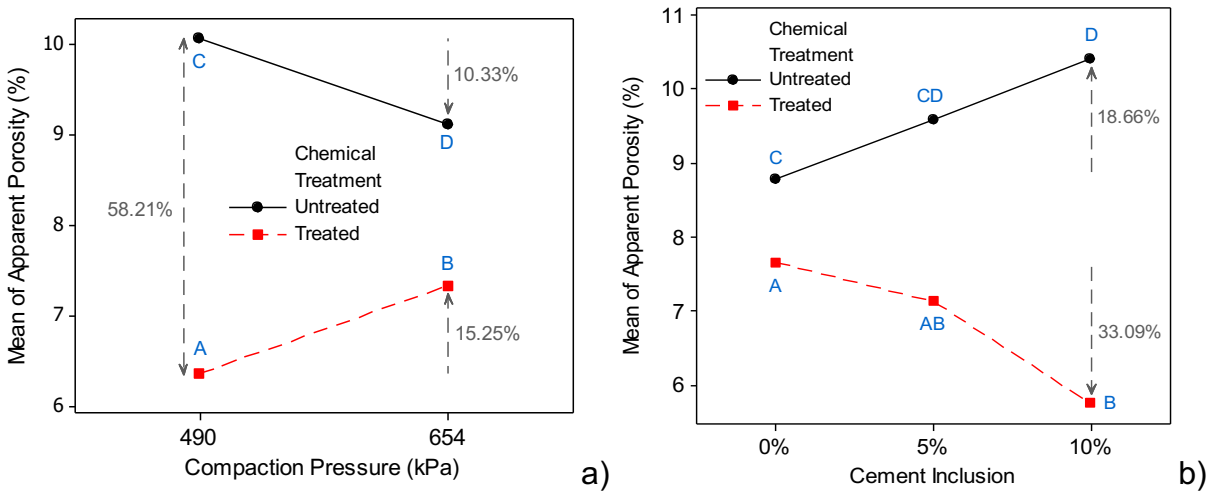

Figure 11. Interaction effect plots of second-order on the mean of the apparent porosity.

Table 7. Amount of expelled resin.

Experimental condition	Cement (%)	Chemical Treatment	Compaction Pressure (kPa)	Expelled resin (g)	Expelled resin (%)
1	0	Treated	654	49.17	17.31%
2	0	Treated	490	39.45	13.89%
3	0	Untreated	654	38.37	13.51%
4	0	Untreated	490	14.00	4.93%
5	5	Treated	654	52.64	17.65%
6	5	Treated	490	38.49	12.91%
7	5	Untreated	654	50.66	16.99%
8	5	Untreated	490	30.55	10.25%
9	10	Treated	654	50.45	16.15%
10	10	Treated	490	22.94	7.34%
11	10	Untreated	654	50.10	16.04%
12	10	Untreated	490	20.48	7.02%

Tensile Strength

The cement inclusions led to a decrease of the tensile strength of the materials fabricated under low compaction (Figure 12a). No difference was observed between the mean values of the samples characterised by 5wt% and 10wt%, as shown by the Tukey test (same A grouping). This result is in accordance to one observed during the matrix characterization, and implies that the cement particles increase the polymer viscosity, which results on a poor fibre wettability and, consequently, low interfacial adhesion. At 654 kPa, the inclusions of particles do not

affect the tensile strength of the hybrid composites. A significant decrease was however observed for the non-particulate composite, which can be attributed to the expelled resin at high compaction. Although the tensile strength of the polymer is lower than the one of the coir fibre, the presence of the matrix is important to guarantee the fibre load transfer.

Figure 12b shows a significant increase in strength when the treated coir fibres were used. This behaviour can be attributed to the removal of impurities and non-cellulosic constituents from the fibre surface and the creation of a rougher topography after alkalinisation, improving the interface quality and the mechanical fibre-matrix interlocking. In addition, sodium hydroxide promotes the exposure of the hydroxyl groups of cellulose, which enhances the chemical bonding between the fibres and the matrix, since the purified fibre surface enables more hydrogen bonds to be formed between the hydroxyl groups of the cellulose at one side, and the epoxy groups at the other side [16, 23, 25].

It is also noticed a slight reduction in strength due to the cement microparticles, which indicates a weaker particle-matrix interfacial adhesion. This is also consistent with the results observed during the matrix characterization (see Table 4). This result also implies the mass content of cement particles used are relatively high.

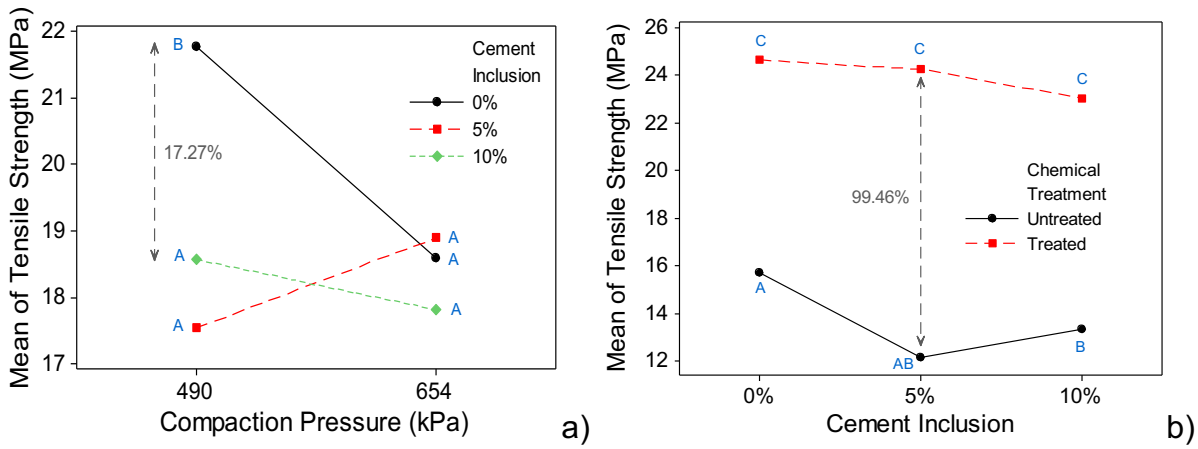

Figure 12. Second-order Interaction effect plots for the mean tensile strength response.

Tensile modulus

Figure 13 shows the main and interaction effect plots related to the tensile modulus. A reduction of 15.57% was noted when the cement particles were incorporated. However, at these levels (5wt% and 10wt%) the elastic moduli were considered equivalents, as highlighted by the same B grouping calculated through the Tukey test.

According to Figure 13b, a substantial increase in stiffness (~75%) was achieved for both pressure levels when the treated coir fibres were used. This behaviour can be explained by the higher coir fibre stiffness (see Table 3) and higher fibre/matrix interfacial adhesion after treatment. The pressure factor did not provide significant changes on the treated composites (C grouping); however, an increase in modulus (29.50%) was observed for the untreated coir fibre composites fabricated at 654 kPa. Such effect may be due to the increase of the effective fibre/matrix contact area and, the consequent enhancement of the mechanical interlocking (as previously discussed).

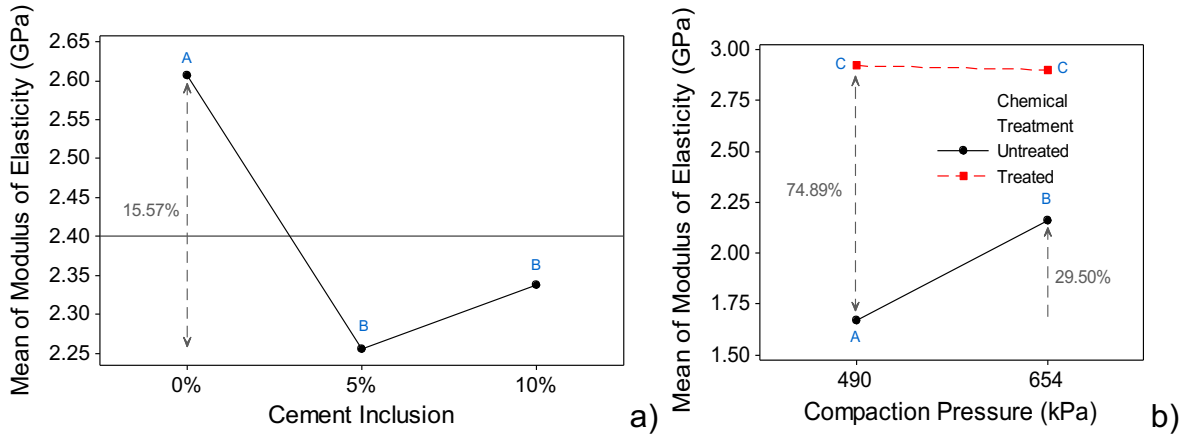

Figure 13. Effect plot of the inclusion of cement (a), second-order interaction of the compaction pressure and the chemical treatment (b) on the modulus of elasticity of the composites.

Flexural strength

Figure 14 shows the third-order interaction effect plot related to the mean flexural strength. The chemical treatment enhanced the flexural strength of the composites because of the good post-treatment fibre/matrix compatibility (Figures

14a and 14b). A reduction in flexural strength was also identified when the cement particles were incorporated to the treated materials (Figure 14a), while non-treated materials did not present significant changes. Some authors [32, 52, 53] have reported an increase in flexural strength, due to the interlocking effect at the interlaminar regions. This effect may not have been probably achieved in our case because of the use of short, randomly oriented coir fibres, and the weak particle-matrix interfacial bonding. Moreover, cement amounts under 5wt% must be the scope of future investigations, especially when short random fibre reinforced composites are designed. The compaction levels considered do not play an important role on the flexural strength of the composites.

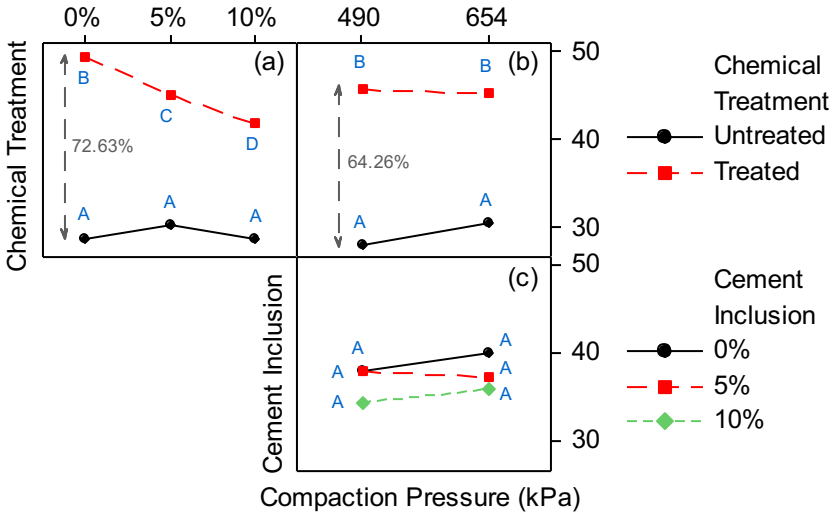

Figure 14. Interaction effect plot of the compaction pressure, cement inclusion and chemical treatment on the flexural strength of the composites.

Flexural Modulus

Figure 15 shows the interaction effect plot related to the flexural modulus. Higher flexural moduli were achieved by composites made of treated fibres and cement particles fabricated at 654 kPa. The cement particles contribute to the increase of the stiffness of the matrix, especially at compressive loadings above the beam neutral axis [32, 33, 53]. The incorporation of 5wt% and 10wt.% of Portland cement microparticles significantly increased by 18%-24% the flexural modulus of coir fibre composites compacted at 654 kPa (Figure 15c). The higher-pressure level provided a better wettability of the fibres and the particles, enhancing therefore the fibre/particle/matrix interfacial adhesion.

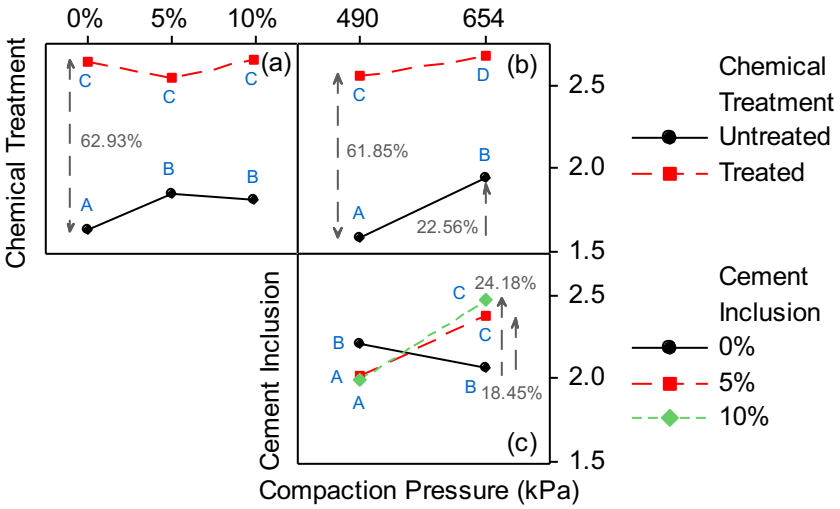

Figure 15. Interaction effect plot of the compaction pressure, cement inclusion and chemical treatment for the flexural modulus.

Impact Resistance

Figure 16 shows the interaction effect plot related to the mean of the impact resistance. The alkaline treatment decreased the impact resistance of the composites (Figures 16a and 16b). According to Albuquerque et al. [54], the impact resistance is very sensitive to the level of bonding and, usually, very strong interfaces have a detrimental effect on the impact properties. In most fibre-reinforced composites, a significant part of energy absorption during impact takes place through the fibre pull-out process. The low impact resistance achieved by the treated coir fibre reinforced composites can be explained by the fracture of the fibres at the plane of crack, with little fibre pull-out [54]. This phenomenon was evidenced by observing the SEM images of the composite cross section (Figure 17). Figure 17a shows a pull-out mechanism present in the untreated fibres, while the Figure 17b exhibits a fracture of treated fibres due to the high fibre/matrix adhesion. Figure 17b also demonstrated a homogeneous distribution of cement particles within the composites.

Figures 16b and 16c show that the higher compaction increased in general the impact resistance, except for the composites made with 10wt% of cement particles. The failure mode under dynamic loading is more affected by the fibre content, instead of the matrix fraction [34]. Thus, this behaviour might be attributed to an increase in the fibre volume fraction caused by the loss of the matrix phase during

the compaction at 654 kPa. The interaction between the cement inclusion and the chemical treatment (Figure 16a) did not provide considerable changes to the response within the range of levels considered. This may be attributed to the weak particle-matrix compatibility that impedes the mechanical load transfer in this interface region. However, a significant interaction was observed between the cement inclusion and the compaction pressure (Figure 16c). This indicates that the fibre-matrix-particle interface bonding is strongly affected by the wettability of the fibres and the mass fraction of cement particles.

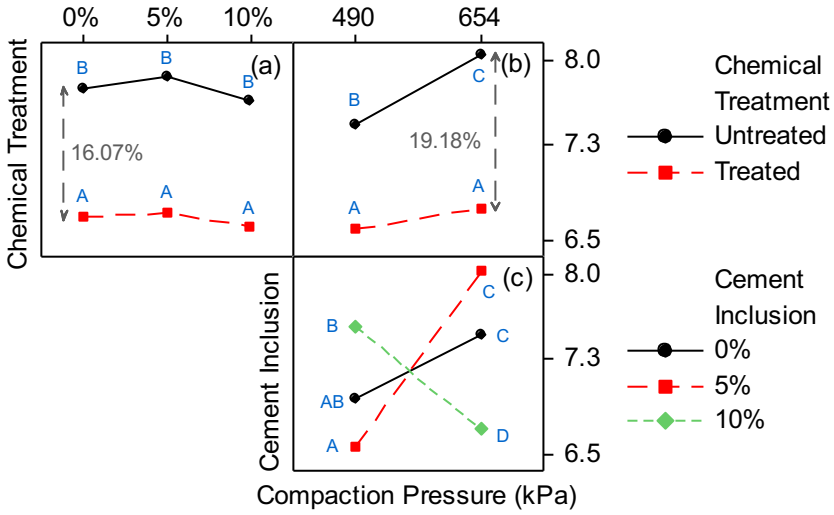

Figure 16. Interaction effect plot of the compaction pressure, the cement inclusion and the chemical treatment for the impact resistance response.

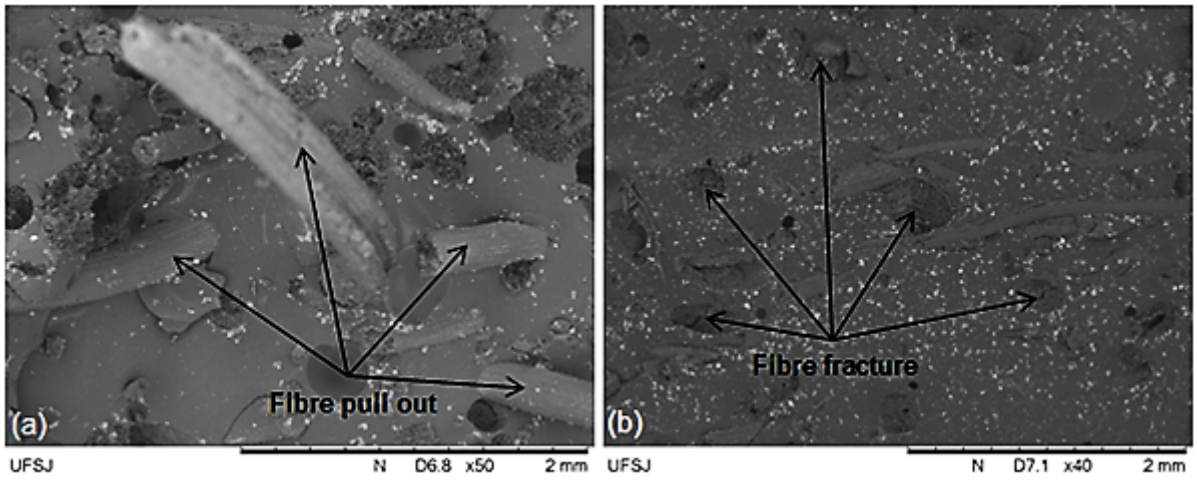

Figure 17. SEM images of the fractured surfaces after impact of the untreated (a) and treated (b) coir fibre composites.

4. Conclusions

The alkali treatment reduced the apparent porosity and significantly improved the tensile and flexural properties of the HSCoirFRCs because of the improved fibre/matrix bonding. However, this strong interface decreased the impact resistance of the materials due to fibre failure. The compacting pressure significantly affected the whole set of the physical properties. In general, the higher level of pressure (654 kPa) enhanced the fibre wettability and, consequently, the mechanical performance of the composites. The use of cement particles led to increased apparent density. The apparent porosity behaved however differently depending on the treatment and pressure levels adopted. The cement microparticles did not prove to be an efficient secondary reinforcement phase under tensile and flexural loading. However, a slight increase in the flexural modulus of the untreated composites was observed, which was attributed to a positive effect under compressive loadings. From these results it is evident that enhanced mechanical and physical properties cannot be achieved simultaneously, and the composite must be designed for a specific set of properties. Nonetheless, the HSCoirFRCs can be considered an economical and sustainable alternative in future lightweight secondary structural parts in different engineering field.

Acknowledgments

The authors would like to thank CAPES (MSc scholarship), CNPq (PP-306767/2016-3) and FAPEMIG (PPM-00075-17) for the financial support and *Deflor Bioengenharia* for the coir fibre supplied.

References

[1] Akil HM, Omar MF, Mazuki AAM, Safiee S, Ishak Zam, Abu Bakar A. Kenaf fiber reinforced composites: A review. Mater Design 2011;32:4107-4121.

[2] Ku H, Wang H, Pattarachaiyakoop N, Trada M. A review on the tensile properties of natural fiber reinforced polymer composites. Compos Part B Eng 2011;42:856-873.

213 [3] Thomas S, John MJ. Biofibres and biocomposites. Carbohyd Polym 2008;71:343-
214 364.
215
216 [4] Tran LQN, Minh TN, Fuentes CA, Truong Chi T, Van Vuure AW, Verpoest I.
217 Investigation of microstructure and tensile properties of porous natural coir fibre for
218 use in composite materials. Ind Crop Prod 2015;65:437-445.
219
220 [5] Abdul Khalil HPS, Bhat AH, Yusra AFI. Green composites from sustainable
221 cellulose nanofibrils: A review. Carbohyd Polym 2012;87:963-979.
222
223 [6] Satyanarayana KG, Sukumaran K, Mukherjee PS, Pavithran C, Pillai SGK.
224 Natural Fibre–Polymer Composites. Cement Concrete Comp 1990;12:117-136.
225
226 [7] Brahmakumar M, Pavithran C, Pillai RM. Coconut fibre reinforced polyethylene
227 composites: effect of natural waxy surface layer of the fibre on fibre/matrix interfacial
228 bonding and strength of composites. Compos Sci Technol 2005;65:563-569.
229
230 [8] Thakur VK, Thakur MK. Processing and characterization of natural cellulose
231 fibers/thermoset polymer composites. Carbohyd Polym 2014;109:102-117.
232
233 [9] Yan L, Su S, Chouw N. Microstructure, flexural properties and durability of coir
234 fibre reinforced concrete beams externally strengthened with flax FRP composites.
235 Compos Part B Eng 2015;80:343-354.
236
237 [10] Yan L, Chouw N. Crashworthiness characteristics of flax fibre reinforced epoxy
238 tubes for energy absorption application. Mater Design 2013;51:629-640.
239
240 [11] Yan L, Chouw N, Jayaraman K. Lateral crushing of empty and polyurethane-
241 foam filled natural flax fabric reinforced epoxy composite tubes. Compos Part B Eng
242 2014;63:15-26.
243
244 [12] Yan L, Chouw N. Experimental study of flax FRP tube encased coir fibre
245 reinforced concrete composite column. Constr build mater 2013;40:1118-1127.
246

[13] Huang L, Yan B, Yan L, Xu Q, Tan H, Kasal B. Reinforced concrete beams strengthened with externally bonded natural flax FRP plates. Compos Part B Eng 2016;91:569-578.

[14] Choudhury A, Saw SK, Sarkhel G. Surface modification of coir fibre involving oxidation of lignins followed by reaction with furfuryl alcohol: Characterization and stability. Appl Surf Sci 2011;257:3763-3769.

[15] Hu Y, Zhang L. Novel lignocellulosic hybrid particleboard composites made from rice straws and coir fibers. Mater Design 2014;55:19-26.

[16] Rahman MM, Khan MA. Surface treatment of coir fibers and its influence on the fiber's physico-mechanical properties. Compos Sci Technol 2007;67:2369-2376.

[17] Lecompte T, Perrot A, Subrianto A, Le Duigou A, Ausias G. A novel pull-out device used to study the influence of pressure during processing of cement-based material reinforced with coir. Constr build mater 2015;78:224-233.

[18] Monteiro SN, Terrones LAH, D'almeida JRM. Mechanical performance of coir fiber/polyester composites. Polym Test 2008;27:591-595.

[19] Wang W, Huang G. Characterization and utilization of natural coconut fibre composites. Mater Design 2009;30:2741-2744.

[20] Nam TH, Ogihara S, Tung NH, Kobayashi S. Effect of alkali treatment on interfacial and mechanical properties of coir fiber reinforced poly(butylene succinate) biodegradable composites. Compos Part B Eng 2011;42:1648-1656.

[21] Rout J, Misra M, Tripathy SS, Nayak SK, Mohanty AK. The influence of fibre treatment on the performance of coir-polyester composites. Compos Sci Technol 2001;61:1303-1310.

[22] Mir SS, Nafsin N, Hasan M, Hasan N, Hassan A. Improvement of physico-mechanical properties of coir-polypropylene biocomposites by fiber chemical treatment. Mater Design 2013;52:251-257.

[23] Yan L, Chouw N, Huang L, Kasal B. Effect of alkali treatment on microstructure and mechanical properties of coir fibres, coir fibre reinforced polymer composites and reinforced-cementitious composites. Constr Build Mater 2016;112:168-182.

[24] Suresh Kumar SM, Duraibabu D, Subramanian K. Studies on mechanical, thermal and dynamic mechanical properties of untreated (raw) and treated coconut sheath fiber reinforced epoxy composites. Mater Design 2014;59:63-69.

[25] Van De Weyenberg I, Chi Troung T, Vangrime B, Verpoest I. Improving the properties of UD flax fibre reinforced composites by applying an alkaline fibre treatment. Compos Part A Appl S 2006;37:1368-1376.

[26] Gu H. Tensile behaviours of the coir fibre and related composites after NaOH treatment. Mater Design 2009;30:3931-3934.

[27] Abot JL, Song Y, Schulz MJ, Shanov VN. Novel carbon nanotube array-reinforced laminated composite materials with higher interlaminar elastic properties. Compos Sci Technol 2008;68:2755-2760.

[28] Fu S.-Y, Feng X.-Q, Lauke B, Mai Y.-W. Effects of particle size, particle/matrix interface adhesion and particle loading on mechanical properties of particulate–polymer composites. Compos Part B Eng 2008;39:933-961.

[29] Silva LJ, Panzera TH, Velloso VR, Christoforo AL, Scarpa F. Hybrid polymeric composites reinforced with sisal fibres ans silica microparticles. Compos Part B Eng 2012;43:3436-3444.

[30] Silva LJ, Panzera TH, Velloso VR, Rubio JCC, Christoforo AL, Scarpa F. Statistical design of polymeric composites reinforced with banana fibres and silica microparticles. J Compos Mater 2012;47:1199-1210.

[31] Panzera TH, Sabariz ALR, Strecker K, Borges PHR, Vasconcelos DCL, Wasconcelos WL. Mechanical properties of composite materials based on Portland cement and epoxy resin. Cerâmica 2010;56:77-82.

[32] Torres RB, Santos JC, Panzera TH, Christoforo AL, Borges PHR, Scarpa F. Hybrid glass fibre reinforced composites containing silica and cement microparticles based on a design of experiment. Polym Test 2017;57:87-93.

[33] Melo ABL, Paiva LFL, Santos JC, Panzera TH, Freire RTS. An statistical analysis of epoxy polymer reinforced with micro ceramic particles. J Res Updates Polym Sci 2016;5:108-113.

[34] Oliveira LA, Santos JC, Panzera TH, Vieira LM, Rubio JCC. Preliminary investigations on short coir fibre reinforced composites. In: 3rd Brazilian Conference on Composite Materials – BCCM3. Brazil, 2016.

[35] ASTM D3822/D3822M-14:2014. Standard Test Method for Tensile Properties of Single Textile Fibers.

[36] ASTM D276-12:2012. Standard Test Methods for Identification of Fibers in Textiles.

[37] ASTM D638-14:2014. Standard Test Method for Tensile Properties of Plastics.

[38] ASTM D790-15e2:2015. Standard Test Methods for Flexural Properties of Unreinforced and Reinforced Plastics and Electrical Insulating Materials.

[39] ASTM D695-15:2015. Standard Test Method for Compressive Properties of Rigid Plastics.

[40] ASTM D6110-10:2010. Standard Test Method for Determining the Charpy Impact Resistance of Notched Specimens of Plastics.

[41] ASTM D3039/D3039M-14:2014. Standard Test Method for Tensile Properties of Polymer Matrix Composite Materials.

[42] Anggraini V, Asadi A, Huat BBK, Nahazana, H. Effects of coir fibers on tensile and compressive strength of lime treated soft soil. Measurement 2015;59:372-381.

[43] Defoirdt N, Biswas S, De Vriese L, Tran LQN, Acker JV, Ahsan Q, Gorbatikh L, Van Vuure A, Vespoest I. Assessment of tensile properties of coir, bamboo and jute fibre. Compos Part A Appl S 2010;41:588-595.

[44] Munawar SS, Umemura K, Kawai S. Characterization of the morphological, physical, and mechanical properties of seven nonwood plant fiber bundles. J Wood Sci 2007;53:108-113.

[45] Silva GG, De Souza DA, Machado JC, Hourston DJ. Mechanical and Thermal Characterization of Native Brazilian Coir Fiber. J Appl Polym Sci 2000;76:1197-1206.

[46] Geethamma VG, Mathew T, Lakshminarayanan R, Thomas S. Composite of short coir fibres and natural rubber: effect of chemical modification, loading and orientation of fibre. Polymer 1998;39:1483-1491.

[47] Rosa MF, Chiou B, Medeiros ES, Wood DF, Williams TG, Mattoso LHC, Orts WJ, Imam SH. Effect of fiber treatments on tensile and thermal properties of starch/ethylene vinyl alcohol copolymers/coir biocomposites. Bioresource Technol 2009;100:5196-5202.

[48] Essabir H, Bensalah, MO, Rodrigue D, Bouhfid R, Qaiss A. Structural, mechanical and thermal properties of bio-based hybrid composites from waste coir residues: Fibers and shell particles. Mech Mater 2016;93:134-144.

[49] Marques AR, Patrício PSO, Santos FS, Monteiro ML, Urashima DC, Rodrigues CS. Effects of the climatic conditions of the southeastern Brazil on degradation the fibers of coir-geotextile: Evaluation of mechanical and structural properties. Geotext Geomembranes 2014;42:76-82.

[50] Montgomery DC, Runger GC. Applied Statistics and Probability for Engineers, 6th. ed. New York, NY, USA: John Wiley & Sons, 2014.

[51] Wu CFJ, Hamada MS. Experiments: planning, analysis, and parameter design optimization. New York, NY, USA: John Wiley & Sons, 2000.

[52] Haque A, Shamsuzzoha M. S2-glass/epoxy polymer nanocomposites: manufacturing, structures, thermal and mechanical properties. J Compos Mater 2003;37:1821-1837.

[53] Detomi AC, Santos RM, Ribeiro Filho SLM, Martuscelli CC, Panzera TH, Scarpa F. Statistical effects of using ceramic particles in glass fibre reinforced composites. Mater Design 2014;55:463-470.

[54] Albuquerque AC, Joseph K, Carvalho LH, D'almeida JRM. Effect of wettability and ageing conditions on the physical and mechanical properties of uniaxially oriented jute-roving-reinforced polyester composites. Compos Sci Technol 2000;60:833-844.